

Marrella et al.:

# ***In Vitro* Demonstration of Intestinal Absorption Mechanisms of Different Sugars Using 3D Organotypic Tissues in a Fluidic Device**

## **Supplementary Data**

### **Theoretical and Computational Fluid Dynamics (CFD) analysis**

Firstly, a theoretical model was developed, starting from the geometry of the MIVO<sup>®</sup> device to calculate the flow rate to set in the peristaltic pump for obtaining a capillary velocity beneath the EpilIntestinal tissue model. The 3D domain, the related size and dimensions were calculated based on the real dimensions of the circuit used during the tests.

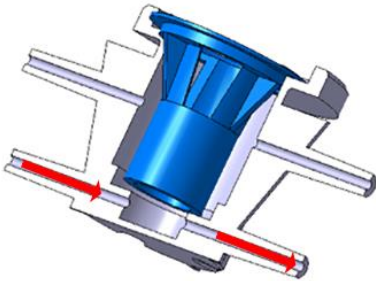
Successively, after reproducing the geometry through a commercial software, the fluid dynamics within the MIVO<sup>®</sup> chamber were modelled by using the *Laminar Fluid Flow module* of Comsol Multiphysics 5.3a. The fluid was assumed to be laminar and incompressible, and the fluid profile was based on Navier-Stokes equations (1a, 1b):

$$\rho \left( \frac{\partial u}{\partial t} + u \cdot \nabla u \right) = -\nabla p + \mu \nabla^2 u \quad (\text{Equation 1a})$$

$$\rho(\nabla \cdot u) = 0 \quad (\text{Equation 1b})$$

where  $u$  is the fluid velocity and  $p$  the fluid pressure across the system. The density  $\rho$  and dynamic viscosity  $\mu$  values were approximated with those of water.

**A**



**B**

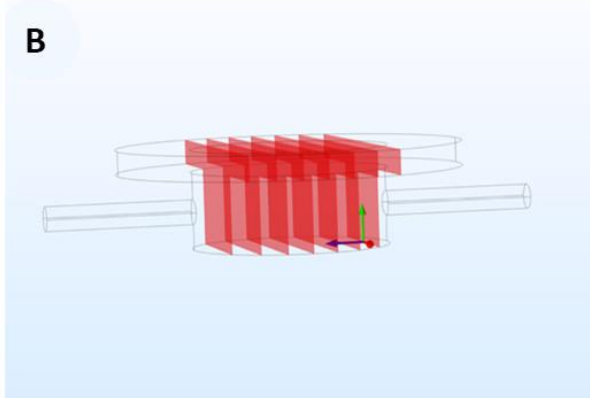


**Fig. S1: Geometry of MIVO<sup>®</sup> device and plane sections used in CFD analysis**

(A) Geometry of the MIVO<sup>®</sup> device; red arrows indicate the flow direction; (B) the plane sections considered in the CFD analysis within the MIVO<sup>®</sup> chamber. The reference system is set beneath the EpilIntestinal tissue model, where the fluid flow was modelled.

Figure S2 shows the velocity module in the MIVO<sup>®</sup> chamber at the different flow rates. The flow rate 2.3 mL/min was chosen for experiments to achieve capillary velocities.

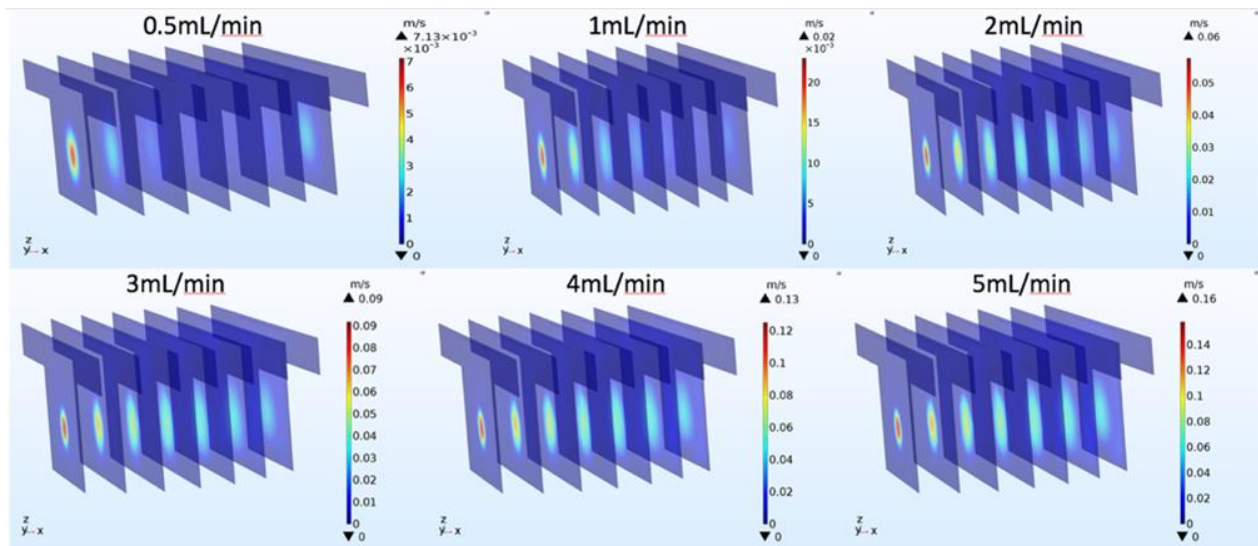


**Fig. S2: Velocity profiles at different flow rates within the MIVO<sup>®</sup> chamber**

#### **FE-SEM analysis of EpilIntestinal tissue model after lactulose absorption test**

As shown in Figure S3, sugar crystals remain deposited over the surface of the villi present in the EpilIntestinal tissue model.

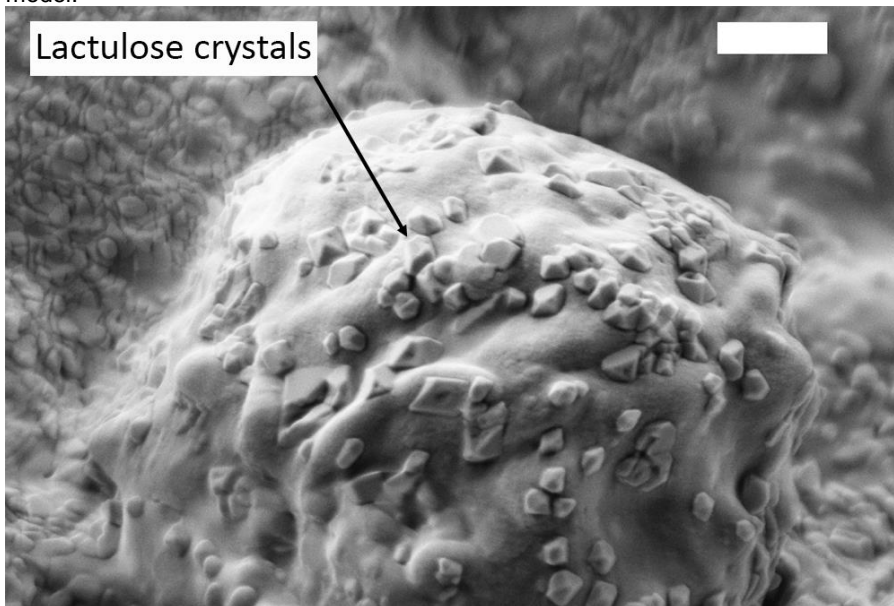


**Fig. S3: FE-SEM analysis of intestinal tissue after lactulose absorption test within MIVO<sup>®</sup> chamber showing an intestinal villus**

Bar is 1  $\mu$ m.

### Sugar absorption test in static conditions

Sugar absorption tests were repeated in static conditions. As shown in Figure S4 the percentage of absorbed mannitol was much greater than that of lactulose for each time point, as in dynamic conditions. Although a slight reduction of the amount of lactulose passed in static conditions can be observed, a statistical analysis between the amount of both sugars passed in static and dynamic conditions showed no significant differences for each experimental time point ( $P > 0.05$ ).

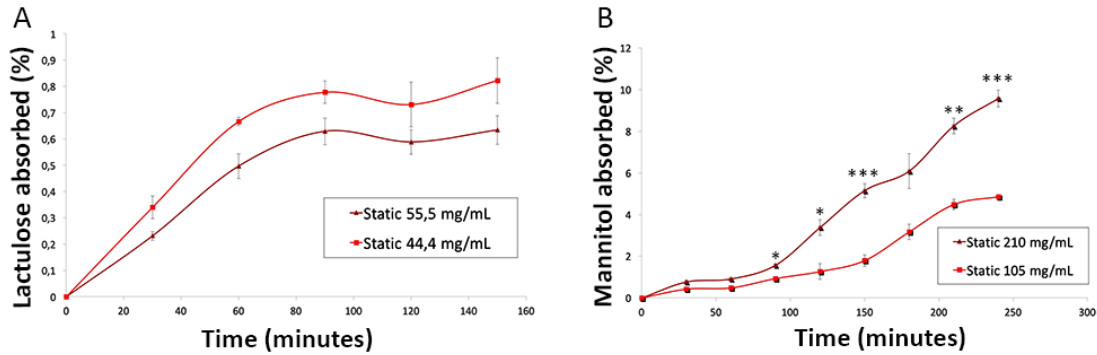


**Fig. S4: Comparison of the absorption of two different concentrations of lactulose (A) and mannitol (B) in static conditions**

Values are presented as mean  $\pm$ SEM. N = 6. Student's *t*-test. \* $P < 0.05$ ; \*\* $P < 0.01$ ; \*\*\* $P < 0.001$ .

### Lactulose absorption test at a lower concentration

Sugar absorption tests were repeated in dynamic conditions with a lower lactulose concentration in the donor chamber (33.3 mg/mL). As shown in Figure S5, the percentage of sugar absorbed is around 1%, consistent with the values obtained with the other concentration tested (55.5 mg/ml and 44.4 mg/mL). This confirms that the amount of sugar passed is not dose-dependent, different from mannitol.

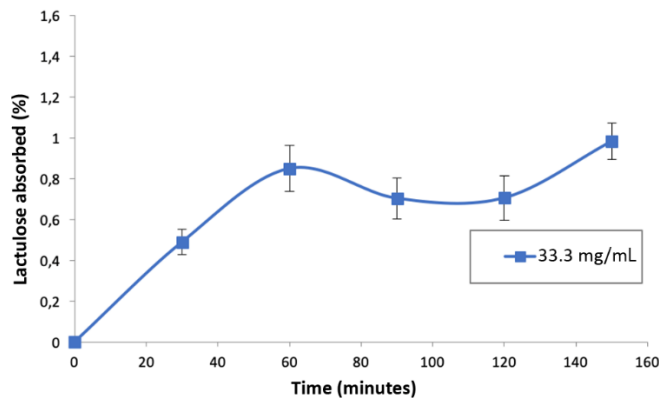


**Fig. S5: Absorption of lactulose in dynamic conditions**

Values are presented as mean  $\pm$ SEM. N = 6. Student's *t*-test. \* $P < 0.05$ ; \*\* $P < 0.01$ ; \*\*\* $P < 0.001$ .

### Drug permeation tests

To confirm that the permeability of compounds in the 3D intestinal tissue model correlates with that of historical human absorption, we used four model drugs representing either low ( $\leq 60\%$ ) or high ( $\geq 80\%$ ) absorption in humans. The samples of donor and receiver side transport buffers from the permeability experiments using healthy and untreated 3D intestinal tissues were analyzed using LC/MS/MS as described previously (Ayehunie et al., 2018).

The apparent permeability coefficient ( $P_{app}$ ) was calculated according to the equation:

$$P_{app} = \frac{dQ/dt}{C_0 \times A}$$

where  $dQ/dt$  is the rate of permeation,  $C_0$  is the initial concentration of test agent, and  $A$  is the area of the monolayer or tissue ( $A = 0.6 \text{ cm}^2$  of the 3D intestinal tissue).

As shown in Table S1, the highly permeable drugs showed a  $P_{app} > 2 \times 10^{-6} \text{ cm s}^{-1}$  and the two low permeable drugs showed a  $P_{app} < 2 \times 10^{-6} \text{ cm s}^{-1}$ . Although the mechanisms of compound permeation through intestinal tissue are not completely understood, there appears to be a similarity of the 3D small intestinal tissue to the *in vivo* counterpart in terms of structure, barrier properties, and expression of transporters and metabolizing enzymes.

**Tab. S1: Drug permeability results using Epilntestinal tissue model for two drugs with lower and two drugs with higher known permeability**

Average (N = 2-5 experiments); assay duration = 2 h

Test Article	$P_{app}$ ( $10^{-6} \text{ cm s}^{-1}$ )	% Hu Absorption	BCS Classification	No. lot repeats
Omeprazole	12.2 $\pm$ 5.21	80	II	N = 3
Carbamazepine	19.7 $\pm$ 1.87	90	II	N = 3
Acyclovir	1.4 $\pm$ 0.82	30	III	N = 3
Metformin	1.3 $\pm$ 0.52	60	III	N = 4